Noble metal alloy clusters in the gas phase derived from protein templates: Unusual recognition of palladium by gold

Ananya Baksi and T. Pradeep*

DST Unit of Nanoscience (DST UNS) and Thematic Unit of Excellence, Department of Chemistry, Indian Institute of Technology Madras, Chennai 600036, India.

Abstract

Matrix assisted laser desorption ionization of a mixture of gold and palladium adducts of the protein lysozyme (Lyz) produces naked alloy clusters of the type $Au_{24}Pd^{+}$ in the gas phase. While lysozyme-Au adduct makes Au_{18}^{+}, Au_{25}^{+}, Au_{38}^{+} and Au_{102}^{+} ions in the gas phase, lysozyme-Pd alone does not make any analogous cluster. Addition of various transition metal ions (Ag^{+}, Pt^{2+}, Pd^{2+}, Cu^{2+}, Fe^{2+}, Ni^{2+} and Cr^{3+}) in the adducts contribute to drastic changes in the mass spectrum; but only palladium makes alloys in the gas phase. Besides alloy formation, palladium enhances the formation of specific single component clusters such as Au_{38}^{+}. While other metal ions like Cu^{2+} help forming Au_{25}^{+} selectively, Fe^{2+} catalyzes the formation of Au_{25}^{+} over all other clusters. Gas phase cluster formation occurs from protein adducts where Au is in the 1+ state while Pd is in the 2+ state. The creation of alloys in the gas phase is not affected whether a physical mixture of Au and Pd adducts or a Au and Pd co-adduct is used as the precursor. The formation of Au cores and AuPd alloy cores of the kind comparable to monolayer protected clusters imply that naked clusters themselves may be nucleated in solution.

1 Introduction

Monolayer protected sub-nanometer clusters of noble metals having precise composition are some of the most fascinating materials of current research.[1-5] Intense luminescence, unusual catalysis, novel physical properties (such as magnetism) have made these systems subjects of passionate research. Despite the discovery of numerous clusters with diverse composition,[6-26] only four clusters, namely, $Au_{25}(SR)_{18}$,[7,11] $Au_{38}(SR)_{24}$,[23] $Au_{102}(SR)_{40}$,[24] and most recently $Au_{36}(SR)_{24}$[26] have been crystallized so far. The possibility to modify the composition by alloying the core has been explored in several cases. Recently, $Au_{24}Pd(SR)_{18}$[27] and $Au_{36}Pd_2(SR)_{24}$[28] have been characterized. Along with monolayer protected clusters, analogous systems with macromolecular protection, especially in protein templates, have also been made.[29-48] Bovine serum albumin (BSA)[29-36], lactoferrin (Lf)[37,38], lysozyme (Lyz)[39-44] and some other proteins like insulin[45] are used for these kind of studies, among which BSA is most thoroughly studied. Cluster cores composed of Au_{25} and Au_{13} are most stable in larger proteins like BSA[29] and Lf[37,38] whereas fairly smaller Au_{10} core is being stabilized by Lyz.[43] Analogous clusters of Ag[31] and recently, Cu[46] clusters have been investigated, although less commonly. Alloys of Au and Ag[36] with distinct composition have also been prepared in proteins like BSA. Utilization of these clusters using their enhanced luminescence due to Föster resonance energy transfer (FRET) and biocompatibility due to the presence of proteins, along with the specific molecular affinity have made them promising for biolabelling applications[30,45] and specific molecular sensing.[40]

While protected clusters have been many, the naked analogues of them, i.e. clusters without protection have not been seen in mass spectrometric investigations of gas phase clusters. In other words, while $Au_{25}(SR)_{18}$ is known to be stable, its gas phase analogue, naked Au_{25} has not been observed. This is true for all the clusters belonging to this category. Creation of clusters with unusual stability in gas phase experiments requires the aggregation and stabilization energy to be removed efficiently. It has been seen recently that this is indeed possible by the use of protein templates, in laser desorption and ionization experiments.[44] These investigations show the formation of gas phase clusters of naked metal cores of magic numbers such as Au_{18}^+, Au_{25}^+, Au_{38}^+ and Au_{102}^+, where cluster formation is proposed to occur in the vicinity of protein, in the gas phase.

Such observations suggest the possibility of creating naked alloy cores of specific composition in similar experiments. In this paper, we report the formation of naked alloy cores of specific nuclearity in the gas phase, derived from lysozyme and metal ion-catalyzed enhancement of specific cluster cores. Among a number of metals investigated (Ag, Pt, Pd, Cu, Fe, Ni and Cr), only palladium (Pd) is shown to create alloy cores similar to the ones seen in monolayer protected clusters. A new cluster core is also observed with Pd. The results reiterate the possibility to create stable unprotected alloy cluster nuclei using macromolecular templates. Presence of Pd ion in the system catalyzes the formation of Au_{38}^{+} when incubated for 48 hours. Peak positions remain essentially the same in the case of positive and negative ion modes. We have also studied the effect of ionization method on the number metal ion attachment to protein and found that the observed affinity is different when the ionization method is changed from ESI to MALDI. Similar peaks are observable whether Au and Pd adducts are mixed together to get the precursor or Pd^{2+} salt is directly added to Au-Lyz adduct. Specific metal ions can enhance formation of Au_{25}^{+}. Here we propose plasma reaction in the gas phase between ions and molecules in the plasma. The deposition of such clusters on active substrates can create novel catalysts for examining elementary catalytic processes.

2 Experimental

2.1 Materials

Tetrachloroauric acid trihydrate ($HAuCl_4.3H_2O$) was prepared in our laboratory starting from pure gold. Lysozyme, extracted from chicken egg white (>90% purity), and sinapic acid used as MALDI MS matrix were purchased from Sigma Aldrich. Palladium chloride ($PdCl_2$) was purchased from Rankem. All the chemicals were used without further purification. Deionized water was used throughout the experiment.

2.2 Synthesis of metal adducts

When metal ions are added to the protein solution, they are uptaken by the amino acids of the protein and form adducts or complexes. In the case of addition of Au^{3+} to protein, it results in the formation of an Au^{+}-Protein adduct as seen in X-ray photoelectron spectroscopy.[38] Further reduction of this gold bound protein complex in basic condition produce solution phase luminescent quantum clusters.[29] Here we have restricted our study up to the complex formation

step. Solution phase cluster formation has been studied elsewhere.[43] The metal-protein adducts were prepared in two different ways:

a) Au-Lyz and Pd-Lyz adducts were prepared by mixing Lyz and the specific metal salts to get a final concentration of 1.5 mM Lyz and 5 mM in terms of metal ions and incubating the mixture for 2 hours. The resulting adducts were mixed together in different concentration ratios (Au:Pd = 1:3, 1:1 and 3:1) and incubated for 4 hours and the resultant product was subjected to MALDI MS analysis. These samples are labeled as Au-Pd mixed adduct. Best result was obtained for the 3:1 Au:Pd mixed adduct.

b) For the other case, first, the Au-Lyz adduct was prepared as above mentioned way by mixing Au^{3+} and Lyz followed by incubating the mixture. To this adduct, different volumes of $PdCl_2$ were added directly to get Au-Lyz:$PdCl_2$ ratios of 5:1, 5:2, 5:3, and 5:4. The resultant mixture was further incubated for four hours and subjected to MALDI MS study. These samples are labeled as Au-Pd co-adduct.

2.3 Spectrometric analysis and instrumentation

MALDI MS analysis

Experiments were conducted in a matrix assisted laser desorption ionization time-of-flight (MALDI TOF) spectrometer. For this, an Applied Biosystems Voyager-De Pro MALDI TOF instrument was used. The spectra were collected in the m/z range of 2000-100,000 using a N_2 laser at 337 nm. For acquiring each spectrum, a minimum of 100 laser shots were fired and the data were averaged. Laser power was kept at slightly higher value than the threshold power for this system (threshold laser power for these systems is about 1800 in terms of the instrumental unit, we have kept the power at 2200). Minimum delay time used was 10 ns and the maximum was 1500 ns for a delay time-dependent experiment. For all other experiments, delay time was kept at 1000 ns. The samples probed were protein-metal conjugates or adducts of specific composition. Laser induced desorption-ionization and associated chemistry produced naked clusters in the gas phase. Instrumental resolution was $\Delta m/z = 2$ Da in the range investigated. All the compositions were compared with their isotope patterns. Sinapic acid was used as matrix for these experiments. To 10 mg of sinapic acid, 1 mL of 0.1% trifluoroacetic acid (TFA) and acetonitrile mixture (3:1) was added. For spotting, 100 µL of matrix was mixed well with 5 µL

of the sample to be analyzed and spotted to get a dried droplet. Same procedure was repeated at least for three different sets for each sample (prepared separately) to check the reproducibility. All the instrument parameters are listed below for linear positive mode and are applicable for the specific instrument used:

Instrument mode: Linear, positive

Delay time: 1000 ns (minimum is 10 ns)

Laser intensity: 2200 (instrumental unit)

Mass range (Da): 2,000-100,000

Low mass gate (Da): 500

Calibrated for matrix: Sinapic acid

Voltages:

Accelerating: 2000 V

Grid: 87 (0.0-99.9% is the instrument range)

Grid wire: 0.03 (0.000-0.300% is the range)

ESI MS analysis

For the solution phase study, electrospray ionization mass spectrometry (ESI MS) was carried out. For this experiment, an Applied Biosystems 3200 QTRAP LC/MS/MS was used. Spectra were collected in the m/z range of 500-1700 and data were averaged for 100 scans. Declustering and entrance potentials were optimized at 50 and 10 V, respectively. As prepared Au, Pd and mixed adducts were used for this purpose. All the spectra were collected in positive ion mode. 10 µL of TFA was added to 1 mL of these solutions to enhance ionization. Spectra were deconvoluted using Magtran software to get singly charged species from a series of multiply charged spectra (for Lyz, the parent spectrum contains +9 - +12 charge states in the m/z window investigated).

XPS analysis

XPS analysis was done using Omicron ESCA probe spectrometer and polychromatic Mg Kα (hν = 1236.6 eV) was used as the ionization source. Curves were smoothed and fitted using the CasaXPS software. For this analysis, 3:1 Au-Pd mixed adduct of Lyz was used.

SEM/EDAX analysis

Scanning Electron Microscopic (SEM) and Energy Dispersive Analysis of X-rays (EDAX) images were collected using FEI QUANTA-200 SEM instrument.

3 Results and Discussion

3.1 Gas phase gold-palladium alloy formation

For our study, we have used a small protein lysozyme (Lyz, molecular weight 14.3 kDa) as the template for gas phase alloy cluster formation. It contains 129 amino acid residues among which eight are cysteines forming 4 disulphide bonds. Overall size of the protein is around 4 nm and contains 49% helical structure. Structure and position of the cysteines and disulphide bonds are presented in Fig. S1. This helical structure is greatly affected by the breakage of disulphide bonds and an overall 28% loss in helicity was observed in previous study upon cluster formation.[43] Unlike other proteins, Lyz mass spectrum is dominated by its monomer as well as aggregates. For example, Lyz^+ appears at 14.3 kDa, whereas Lyz_2^+, Lyz_3^+, Lyz_4^+ appear at 28.6, 42.9, 57.2 kDa, respectively. Once metal ions like Au^{3+} is added to the system, amino acids reduce Au^{3+} to Au^+ and metal-protein adducts form. Adducts form when Pd^{2+} too is added to the system. These transition metals have higher affinity towards sulphur; therefore it is obvious that, M-S bond will be formed. By this process, disulphide bond has to break to accommodate multiple metal ions inside the protein. For the Au^{3+} addition, we have seen a maximum 10 Au attachments to protein[44], which implies that there are other binding sites also present in the system like carboxyl or amine groups. When both Au and Pd adducts are mixed together as described in 2.2, they form a mixed adduct. These adducts are subjected to MALDI MS analysis and corresponding mass spectra were collected. Fig. 1 compares the positive ion MALDI MS spectra of Au adduct of Lyz with those of mixed Au and Pd adducts and parent Lyz. In the full mass range, Lyz shows a series of peaks attributed to Lyz^+, Lyz_2^+, Lyz_3^+, etc. In the lower mass region (m/z 2000-11000), the spectrum is dominated by the +2 charge state, no other charge state or fragments were observed. As before, the Au adduct shows bare cluster cores with specific

number of atoms like Au_{18}^{+}, Au_{25}^{+}, Au_{38}^{+} and Au_{102}^{+}.[44] These peaks appear with additional features separated by one gold atom and they may be represented as $Au_{18\pm n}^{+}$, $Au_{25\pm n}^{+}$, etc. (n = 0, 1, 2,...). In all of the clusters, the cores try to achieve electronic stability by accruing electrons from ligands and this is shown in the form of sulfur addition peaks for specific clusters like $Au_{18}S_4^{+}$.

In the mass spectrum of the Au-Pd adduct, besides the peaks observed for Au, new peaks attributed to alloys are also observed. These are particularly seen in the case of cluster ions of Au_{18} and Au_{25}. While the cluster region of Au_{38} does not show any alloy formation, the peak intensity is greatly enhanced in comparison to the Au adduct. The spectrum in the Au_{18} and Au_{25} region show markedly different distribution. While Au_{18}^{+} and Au_{25}^{+} were the most intense features in the parent adduct, the alloy ions exhibit a completely different intensity pattern possibly due to their different stability. All the assigned peaks match well with their calculated spectra as represented in Fig. 1 inset. In the Au_{18}^{+} region, a series of peaks appear in an envelope starting from $Au_{16}Pd^{+}$ and continues up to $Au_{19}Pd^{+}$. The very next peak appears with another Pd attached to it. In this envelope, $Au_{20}Pd_2S^{+}$ is the most intense peak. After $Au_{22}PdS^{+}$, this envelope overlaps with the Au_{25}^{+} region. Starting from $Au_{23}Pd^{+}$, the envelope continues with Pd attachment with a few sulfur additions. Unlike in the solution phase, where $Au_{24}Pd(SR)_{18}$ is found to be most stable[27], $Au_{27}Pd^{+}$ shows the highest intensity in the gas phase, although neighboring peaks do not vary much in terms of abundance. This implies nearly equal stability of the alloy cores in that region in the gas phase.

Interestingly, the Au_{38} region does not show any Pd attachment. Although it is possible to get $Au_{36}Pd_2(SR)_{24}$[28] by doping Pd to Au_{38} in the solution phase, using protein template, it is not easy to get the same core in gas phase as protein allows Au_{38}^{+} to acquire structural and electronic stability as already discussed above. One extra envelope appears after the Au_{38} region which was not present in the case of Au adduct. Here, $Au_{47}PdS_2^{+}$ is having the maximum intensity. Other peaks with Pd doping have also been observed, although the intensities do not differ much. It should be noted that, Au_{47}^{+} is not a magic number core neither by the number of core atoms nor by electron count and it was not observed with Au-Lyz adduct. So presence of Pd helps in the formation of metastable cluster cores in the gas phase through the interaction with protein. The same sample was analyzed in linear negative mode too. Peak positions remain

essentially the same in negative ion mode also although there is slight change in their intensity distribution. No new peak appears in this case (Fig. S2).

We have also conducted laser intensity-dependent study to check whether there is any role of laser intensity in the formation of these clusters. The threshold laser intensity is the minimum intensity where we can see appearance of the specific peaks. It is often a practice to keep the experimental laser intensity slightly higher than the threshold intensity to avoid laser induced damage and at the same time get good quality data. In our case, threshold laser intensity was found to be 1800 in terms of the instrumental unit (details of experimental parameters are given in experimental section under MALDI MS analysis sub-section). At the minimum laser intensity (i.e., threshold intensity) also we can see the same peaks as described above for 3:1 Au:Pd mixed adduct. We have slowly increased the intensity to 2600 with an increment of 200 step size (Fig. S3). Peak positions remain the same as well as the intensity distribution for all the laser intensities studied. Best spectrum was observed with a laser intensity of 2200 and the same was used for all the other studies.

Formation of specific cores can be explained in terms of the enhanced stability of such cores in the gas phase. Au_{25}, Au_{38} systems are known to have magic number stability through closed shell electronic structure. Magic number configuration (n*) requires a certain number of delocalized electrons like n*= 2, 8, 18 (20), 34 (40), 58, 92, etc. For example, Au_{38} contains 38 delocalized electrons and hence is not a magic number. To achieve magic number stability, it has to lose 4 electrons which is possible by interacting with the protein. The key observation from a theoretical calculation reported before[44] predicts that these clusters formed in the gas phase namely, Au_{25}^{+}, Au_{38}^{+} etc. do not have magic number to begin with but require the removal of n-n* = 5, 4 electrons, respectively to achieve it.[44] This is possible through the interaction with the cystines (dimeric cysteine). We have calculated the interaction with only the cystine part of the protein, as simulating the whole protein is really difficult. When one cystine (S-S bond) breaks on the cluster surface, two cysteins form and the cluster core loses two electron by this process. For Au_{38}^{+} system, it requires interaction with two cystines to lose 4 electrons and become 34 electron system and to achieve magic number stability. By this process, a HOMO-LUMO gap of Δ_{HL}=0.48 eV opens up and the cluster gets electronic stabilization

whereas for the neutral Au_{38} cluster, Δ_{HL}=0.0 eV. This is also reflected in their calculated structures.

From this part of study, it can be concluded that Pd forms alloy with gold in the gas phase and it also facilitates the emergence of metastable clusters in the gas phase. It is noted that very small gas phase Au-Pd alloys have been reported.[49,50] Incorporation of a single Pd to Au cluster core enhances its catalytic activity tremendously.[49]

3.2 Unusual recognition of palladium by gold in the gas phase

As discussed in the previous section that, Pd is recognized by Au in the gas phase. There are several metals known to form alloys with gold in bulk as well as in the nanosize regime, like Ag, Cu, Pt, etc. In Fig. 2, we present the mass spectra with different metal ions spanning the 3d, 4d and 5d elements which are typically known to form alloys with gold. As we can see, only in the case of Pd, distinct alloy formation is noticed and in this spectrum we mark a region with a black rectangle to show the difference. Au-Lyz and M-Lyz (M = Ag, Pt, Pd, Cu, Ni, Cr and Fe) adducts were mixed together in 3:1 ratio and a MALDI MS study was carried out. With the addition of Pt-Lyz adduct, nearly all the peak positions remain the same but the envelope changes and the $Au_{18}S_4^+$ region becomes more intense than the Au_{25}^+ region. $Au_{19}S_4^+$ peak splits into two, separated by 100 mass units (Fig. S4). Peak at m/z 3839 can be assigned as $Au_{19}S_3^+$ and the next peak at m/z 3935 can be attributed to $Au_{19}S_6^+$, considering no alloy formation with Pt. Since atomic weight of Pt and Au are very close, it is difficult to decide whether any alloy formation has happened or not in this case. Ag is well known to form both solution phase Ag_{QC} and AuAg alloy clusters in proteins and also with monolayer protection. But the gas phase reactivity does not match with the expected solution phase interaction as Ag does not form alloy with Au in similar conditions. Several gas phase Au-Ag alloys have been reported previously.[51-53] Very small cores like Au_mAg_n (m+n=3,5)[51] as well as bigger cores like Au_mAg_n (m+n=19-45)[53] are also studied in the context of gas phase reactivity like binding activity with O_2 and CO for conversion to CO_2. But in the case of our gas phase cluster synthesis using protein templates, without any reducing agent, no alloy formation was observed. Au_{25}^+ intensity gets enhanced in presence of Ag to a greater extent than Au alone but the peak positions remain the same (Fig. S5). Therefore, we can catalytically enhance the formation of Au_{25}^+ in the gas phase from protein template by incorporating Ag in the system. Copper is also known to form alloy with gold and

recently Negishi's group could dope a maximum of five copper atoms in the $Au_{25}(SR)_{18}$ system.[54] In the gas phase, however, a drastic change was found in the overall spectrum upon Cu addition. As Cu is having a high affinity towards sulphur, it occupies Au binding sites in Lyz. This effect is reflected in the main protein peak also where only a few Au attachments are observed. In Fig. S6 inset a, monomer of the Au-Protein adduct and Au-Cu adduct of Lyz are compared. It is clear that in case of Au-Cu adduct, number of Au attachment is less (maximum 10 Au attachments are seen for Au adduct, whereas only two Au attachment is seen for Au-Cu adduct). Same thing is reflected in the aggregates also as marked by green dotted circles. Interesting changes occur in the lower mass region where gas phase bare clusters form. Mass spectrum indicates that exclusively Au_{25}^{+} species form in that range and the shape of the envelope changes (Fig. S6 inset b). So by adding Cu to the gas phase Au precursor, we can selectively get Au_{25}^{+} prior to the mixture of clusters. In presence of 3d transition metals like Ni, Cr and Fe, the intensity of the Au_{25}^{+} region enhances relative to Au_{18}^{+} and Au_{38}^{+} regions, compared to the Au-alone case (Fig. S7-S9). Therefore, catalytic enhancement of Au_{25}^{+} is possible by using these metal ions. This effect is maximum in the case of Fe addition where intensity of $Au_{18}S_4^{+}$ and Au_{38}^{+} region remain same but intensity of Au_{25}^{+} region increases to a greater extent compared to Ni and Cr. In all the cases, $Au_{18}S_4^{+}$ intensity decreases. No alloy formation was observed in any of these cases. This study concludes that Pd is the only metal recognized (selected) by Au in gas phase alloy formation. If we consider electrochemical potential for Au, Pd, Pt, Ag and Cu, standard reduction potentials are as following:

$$Cu^{2+}+e^{-}\rightarrow Cu^{+} \quad E^{0}= 0.159\ V$$

$$Cu^{+}+e^{-}\rightarrow Cu \quad E^{0}= 0.520\ V$$

$$Ag^{+}+e^{-}\rightarrow Ag \quad E^{0}= 0.7996\ V$$

$$Pd^{2+}+2e^{-}\rightarrow Pd \quad E^{0}= 0.915\ V$$

$$Pt^{2+}+2e^{-}\rightarrow Pt \quad E^{0}= 1.188\ V$$

$$Au^{3+}+2e^{-}\rightarrow Au^{+} \quad E^{0}= 1.36\ V$$

$$Au^{+}+e^{-}\rightarrow Au \quad E^{0}= 1.83\ V$$

From these electrode potentials, it is clear that Au^{3+} can be easily reduced to an intermediate Au^{+}-protein complex. It is this Au^{+}-complex that makes the Au clusters in the gas phase which are in Au(0) state. Both Pd^{2+} and Pt^{2+} are having reduction potentials next to Au^{+} and it is likely that Pd^{2+} and Pt^{2+} can be reduced to Pd^{0} and Pt^{0} in the gas phase. But as Pt and Au mass numbers are almost the same, we cannot exactly tell if there is any alloy formation or not with Pt. But Pd and Au mass difference is nearly 90 amu and it is rather easy to distinguish Pd added alloy cluster peaks from the original Au cluster peaks.

3.3 Difference in metal ion binding

From the previous discussion, it is clear that only Pd is recognized by gold in the gas phase. If we see carefully, the binding tendency of these metal ions are completely different from each other. To verify our argument, we have performed a detailed ESI MS and MALDI MS study for each metal adducts of protein, namely, Au, Ag, Pd, and Pt. Same protein to metal ratio (Lyz 1.5 mM and M ion 5 mM) was used to avoid concentration-dependent issues. As we have shown before, with all the concentration of Au^{3+} used, we can see only upto 3 Au attachments to the protein. As there are only 8 cysteines in the protein and Au binding is strongly dependent on number of cysteine residues and hence after a certain Au^{3+} concentration binding sites are saturated. When these adducts were examined using MALDI MS, a maximum of 10 Au attachments were observed and bare clusters were formed as already described. These decrease in number of Au attachment in solution phase mass spectrum (ESI MS) can be attributed to charge-induced dissociation of the high charge states (+8-+12 are normally observable for Lyz and Lyz_2 in positive mode ESI MS).[43,44] Binding of Ag ions to protein is completely different from Au (Fig. S10). For both monomer and dimer region, +8 charge state shows maximum number of Ag attachment (more than 12 Ag attachment is observed). Another interesting observation is that for this specific charge state, two consecutive Ag bound peaks have the same intensity. These 8 Ag attachments can be justified considering 8 cysteines and similar intensity patterns can be due to the breakage of 4 cystine bonds. Once one cystine bond is broken, two Ag can be attached to two different sulphur ends with equal probability and hence the same intensity for two consecutive Ag bound peaks. So, Ag can be attached to cysteines as well as –COOH or NH_2 groups (as more than 8 Ag are attached) but the binding affinity is different. When the same sample is used for MALDI MS analysis, it shows no Ag attachment to it which implies that Ag

is loosely bound to the protein and at the experimental conditions used, it desorbs form the template and we can't see any attachment. We have not seen any gas phase bare Ag cluster either, unlike in the case of Au (Fig. S11). For the Pd-Lyz adduct, we see multiple peaks separated by Pd in the ESI MS analysis. Maximum 8 Pd attachments can be seen clearly in this case (Fig. S12). As Pd has multiple isotopes, the peaks are broader but due to less resolution, each isotope distribution is not separately seen for that charge state. The same sample shows only a single Pd attachment in MALDI MS analysis (Fig. S13) but no gas phase Pd clusters were observed. When Pt-Lyz adducts were studied using ESI MS analysis, a maximum of 6 Pt attachments were observed (Fig. S14). Strangely, odd number Pt attached peak intensities are very poor compared to the even numbered Pt attached peaks which again proves indirectly the breakage of S-S bonds in cystines. Unlike in other metal ions, Pt shows nearly the same number of attachments in MALDI MS also where we see a broad peak separated by 8 Pt from the parent protein peak and free protein peak is not observed in this case. Dimer, trimer, etc. contain multiple of 8 Pt as observed for Au. The peak position remains the same whether we use additional NaOH or $NaBH_4$ (Fig. S15). This confirms strong binding affinity of Pt towards Lyz. From these studies, it is confirmed that metal ion binding affinities are different for each system and the observed spectrum depends strongly on the ionization method used (ESI or MALDI).

3.4 Solution phase studies of Au-Pd mixed adducts

In order to check the possibility of formation of the above mentioned alloy clusters in solution, electrospray ionization of Au, Pd and Au-Pd adducts of Lyz were analyzed. While Au shows limited number of attachment (up to 3) to Lyz, Pd is having multiple attachments to Lyz (up to 8). When these two adducts are mixed together in different ratios like 1:3, 1:1 and 3:1 (with respect to Au and Pd adducts of Lyz, respectively), mixed attachment features appear in the positive ion mode of ESI MS (Fig. 3a). Distinct separations for Au and Pd are observed. As two Pd attachments and one Au attachment fall at nearly the same mass range and also Pd is having multiple isotopes, it is hard to differentiate them. From this solution phase study, we conclude that both Au and Pd can be attached simultaneously to Lyz. However, no naked alloy clusters were seen in solution. This concludes that cluster formation occurs in the gas phase. Lyz as well as metal adducts of Lyz show multiple charge states like +12, +11, +10 and +9 in the mass range studied. Each of these spectra can be deconvoluted to get the molecular ion peaks arising from

these charge states. The deconvoluted spectrum of Au-Lyz shows two peaks due to one and two Au attachments to it, whereas Pd-Lyz shows two peaks due to three and four Pd attachments. When these two adducts are mixed in 3:1 ratio, the deconvoluted spectrum shows multiple peaks including parent protein besides Pd as well as Au attachment peaks and mixed Au:Pd peaks, as shown in Fig. 3b.

3.5 Alloy formation in the solution state

As reported in our previous study, small Au cluster core (Au_{10-12}) can be stabilized inside a single protein Lyz. Here red luminescent Au clusters were prepared by reduction of Au^{3+} to Au^0 in the basic medium. Monomer as well as aggregates show the same kind of cores inside a single protein. As per example, in monomer region, the cluster peak is separated by 10-12 Au atoms depending on the Lyz:Au^{3+} ratio used from the free protein peak and the core is assigned as Au_{10-12}@Lyz. Whereas $(Au_{10-12}@Lyz)_n$ (n=2,3,4,…) are also observable in the whole mass range studied. Addition of extenrnal reducing agent to the basic medium is required to reduce Ag^+ to Ag^0 for forming red luminescent Ag clusters. For our study, we have used 1:4 ratio of Lyz:Ag^+ and the cluster core obtained by this process is assigned as Ag_{13}@Lyz (see Fig.4 inset). Au-Lyz adduct and Ag-Lyz adducts were mixed together in 1:3 and 3:1 ratio and reduced further using $NaBH_4$ to luminescent alloy clusters and the mass spectrum were studied for the same. From the mass spectra it is clear that, by varying Au:Ag adduct ratio, we can control the core composition and this process is also tunable as described earlier from our group for BSA protected Au-Ag alloy clusters.[36] The same procedure was followed for Pd alloy formation also. But only one Pd attachment was observed in this process as shown in the mass spectrum (Fig. S16). So, form this study it is confirmed that, solution phase alloy formation is completely different from gas phase alloy formation. We have observed that, in the gas phase, Au-Ag alloy cannot be formed but the same can be formed by using the solution state co-reduction method. Alloy formation with Pd is also distinctly different from gas phase. This study conclusively proves the specific recognition of Pd over other metals in gas phase.

3.6 Concentration and time dependent studies

Cluster distribution and their intensities are affected by the precursor composition as well as time of incubation. Data presented in Figure 5 show that while the gross features are unaffected with

variation in composition, Au_{38}^{+} intensity is greatly enhanced with the Pd content. Various ratios of Au and Pd adducts of Lyz were used (1:1, 1:3 and 3:1 in terms of Au:Pd adducts), but in the case of 3:1 ratio, peaks are well resolved. Suppression of other clusters and enhancement of Au_{38}^{+} are also seen upon increasing the time of incubation to 48 hours. A catalytic enhancement of Au_{38}^{+} is inferred from the spectra.

3.7 Direct addition of $PdCl_2$

To check whether preformed M-Protein adduct is necessary for alloy formation, we designed our experiment in a slightly different way. To verify the role of Pd precursor in the alloy formation process, $PdCl_2$ was added directly to Au-Lyz adduct and the product was examined in MALDI MS. For this study, $PdCl_2$ was directly added to Au-Lyz in various ratios (Au-Lyz:$PdCl_2$= 5:1, 5:2, 5:3 and 5:4). Gas phase alloy formation was observable with minimum $PdCl_2$ addition also in the Au_{18}^{+} region (Fig. 6), where starting from $Au_{16}PdS^{+}$ to $Au_{19}PdS^{+}$, peaks appear with equal Au spacing. After $Au_{19}PdS^{+}$, the next peak is separated by Pd and assigned as $Au_{19}Pd_2S^{+}$. In this case also, we found $Au_{20}Pd_2S^{+}$ to be the most intense peak in the Au_{18}^{+} region as seen in the case of Au-Pd mixed adduct discussed in 3.1. In the Au_{25}^{+} region, we have a single Pd attachment to the core as we have seen for the previous case. A small hump appears just after the Au_{25}^{+} peak, separated by m/z 106 and attributed to $Au_{25}Pd^{+}$. It is clear that alloy cores remain same in terms of their nuclearity for both the cases. Therefore, it can be said that Lyz can uptake Pd simultaneously in presence of Au also. From the protein template, both the metals come to the gas phase and the alloy was formed. This study again proves gas phase association of Au and Pd to form alloy clusters.

3.8 XPS and EDAX analysis

Once metal salts are added to the protein, amino acid residues reduce metal ions and the protein itself gets oxidized. In the case of Au^{3+} addition to protein, Au^{3+} gets reduced to Au^{1+} by the amino acids in normal condition as previously reported for Au clusters synthesized in Lf. We have used Au-Pd mixed adduct for XPS analysis. In our case also we found that the Au $4f_{7/2}$ binding energy appears at 85.0 eV (Figure 7A) in the protein conjugate confirming that most of the Au^{3+} is reduced to Au^{1+} by the protein. But for Pd, the $3d_{5/2}$ binding energy is at 337.1 eV

(Figure 7B) corresponding to Pd^{2+}. Therefore, amino acids of protein cannot reduce Pd^{2+} to Pd^0 or any intermediate oxidation state in this process. Presence of all the possible elements is proved by the survey spectrum as well as by SEM EDAX (Fig. 7). From this study, we determined the atomic ratios of Au:S:Pd to be 1:3.6:0.6 and the expected ratio is 1:2.4:1 on the basis of components used. From the EDAX mapping, it is confirmed that, Au and Pd are uptaken together by the protein.

3.9 Mechanism of alloy formation and delay time dependence

While cluster is being formed, there is a need to remove the heat of aggregation from the system. This is often practiced using the macromolecular template. Protein being a large molecule has high number of degrees of freedom and can act as a heat reservoir to allow cluster growth in the gas phase. Lyz is a very small protein having only 8 Cys residues. So it is unlikely that Au_{38}^{+} or $Au_{47}PdS_2^{+}$ will form inside a single molecule of Lyz. From XPS study, we have confirmed that, Au^0 or Pd^0 does not exist in the solution at normal reaction condition. Therefore, we propose involvement of plasma in this reaction. Gaseous plasma is produced by heating the sample with laser. This plasma contains ions, molecules, aggregates, protein molecules, Lyz-Au adducts, Lyz-Pd adducts as well as mixed adducts and electrons. In gaseous plasma condition, conformation of the adducts will not be same like in solution phase. Constituents will interact with each other to form larger aggregates. Bare cluster formation and stabilization requires interaction with the protein molecules. This can happen through several unimolecular reactions like:

$$Au_n^{+} + Au_m \rightarrow Au_{n+m}^{+} \qquad m = 0,1,2,\ldots;\ n = 1,2,3,\ldots \qquad (1)$$

$$[Lyz\text{-}Au_m]^{+} + Au_n \rightarrow [Lyz\text{-}Au_{m+n}]^{+} \qquad m = 0,1,2,\ldots;\ n = 1,2,3,\ldots \qquad (2)$$

$$[Lyz\text{-}Au_n]^{+} + Lyz\text{-}Au_m \rightarrow [Lyz\text{-}Au_{n+K}]^{+} + [Lyz\text{-}Au_{m-k}] \quad k(<m)=1,2,...;\ n, m = 1,2,3,... \qquad (3)$$

Equation 3 involves intermolecular metal ion transfer. We know that, when small Au cluster core nucleates, it attracts other Au atoms or ions towards itself through aurophilic interactions and starts growing. For solution phase cluster growth also we see intermolecular metal ion transfer, which is reflected in the regeneration of free protein upon longer incubation time.[38,43]

Same kind of reactions can be written for Pd also. Here we note that, we did not see free Pd clusters in gas phase in our experimental condition. Although, Pd_n clusters are known to exist in gas phase and their reactivity is also studied.[55] Au and Pd ions and adducts are formed simultaneously inside the plasma and can interact with each other to form alloys. Here we note that, we did not see more than two Pd attachments in any case.

$$Au_n^+ + Pd_m \rightarrow Au_nPd_m^+ \qquad m = 0,1,2,\ldots; n = 1,2,\ldots \qquad (4)$$

$$Au_n + Pd_m^+ \rightarrow Au_nPd_m^+ \qquad m = 0,1,2,\ldots; n = 1,2,\ldots. \qquad (5)$$

$$[Lyz\text{-}Au_m]^+ + Pd_n \rightarrow [Lyz\text{-}Au_mPd_n]^+ \qquad m = 0,1,2,...; n = 1,2,\ldots. \qquad (6)$$

$$[Lyz\text{-}Au_n]^+ + Lyz\text{-}Pd_m \rightarrow [Lyz\text{-}Au_nPd_k]^+ + [Lyz\text{-}Pd_{m-k}] \qquad k(<m)=1,2,...;\ n, m = 1,2,... \qquad (7)$$

Besides these, there can be several reactions in which anions and electrons can participate. Similar kinds of mechanism can be extended for negative ions also as same clusters form in the negative mode. In the case of laser irradiation, it is always seen that C-S bond breaks and M_nS_m aggregates form. In our study, we observed cluster cores with sulfur attachment ($Au_{20}Pd_2S^+$, $Au_{47}PdS_2^+$ etc.) which again proves involvement of proteins in cluster formation as there is no other source for sulphur in the system.

This kind of plasma reactions can also happen with large protein aggregates due to the delayed extraction of the ionized species. The finite time lag between laser desorption/ ionization and extraction of ions is referred to as the delay time. Normally, for smaller molecules, shorter delay time is enough to efficiently extract all the ions to the detector but for larger molecules, like proteins, longer delay time is generally used. To check the delay time dependence on the gas phase cluster formation, we have performed the experiment with Au-Lyz adduct. If we allow the plasma to react longer, we may get larger cluster cores or a certain cluster core may form in high abundance. However, we saw that there is actually not much delay time dependence as both the cluster cores as well as protein is small. With varying delay time, the peak positions remain essentially the same. In Fig. 8 delay time dependent-MALDI MS are plotted for Au^+@Lyz adduct and from these spectra, it is evident that no new peaks appear. In the inset, m/z 3000-9000 has been expanded. In this region alone, the peak intensities change with delay time. Thus we conclude that the delay time used for the reaction is sufficient for inter- and intra-molecular reactions to occur within the plasma.

4 Conclusions

The data presented show the existence of naked clusters of specific composition. Incidentally at least one of the cluster cores found, namely $Au_{24}Pd^{+}$ is known to exist in the monolayer protected clusters. Besides these alloy clusters, presence of Pd in the condensed phase enhanced the formation of one component clusters such as Au_{38}^{+}. Results point to the catalytic stabilization of certain cluster nuclei. It is seen that Pd is the most important metal recognized by the naked Au clusters while other metals do not show alloy formation in such condition. Although formation of selective cluster likes Au_{25}^{+} is observed in the case of Cu^{2+} addition, presence of silver enhances the formation of Au_{25}^{+} while Pt^{2+} enhances $Au_{18}S_4^{+}$. Other metal ions used in this study like Fe^{2+}, Ni^{2+}, Cr^{3+} catalyze the formation of the $Au_{25\pm n}^{+}$ envelope. Fe^{2+} is catalyzed most efficiently among the three ions. Clusters are formed from metal adducts in the proteins in which gold is in the 1+ state while Pd in the 2+ state. Unusual recognition of Pd as evidenced by the enhanced formation of Au_{38}^{+} and selective formation of Pd containing alloys, of the kind $Au_{20}Pd_2S^{+}$, $Au_{27}Pd^{+}$, $Au_{47}PdS_2^{+}$suggest the participation of palladium in the growth process. Although Ag is not recognized by Au in gas the phase, it is possible to create luminescent Au-Ag alloy clusters, with tunable composition, in solution. We suggest that naked alloy clusters of this kind derived from macromolecular templates may be deposited on active substrates and used for model catalysis. Microscopy and spectroscopy of such naked clusters formed in the gas phase will be interesting.

Supplementary information Available: Supplementary information for this article is available on the internet or from the author.

Author information

Corresponding Author

Address correspondence to pradeep@iitm.ac.in; Fax: + 91-44 2257-0545.

Acknowledgment

A.B. and T.P. thank the Department of Science and Technology, Government of India for continuous support our of research program on nanomaterials. A.B. thanks Council of Scientific and Industrial Research (CSIR) for fellowship. A.B. thanks Mr. M S Bhootaraju for XPS and Ms. Shridevi S Bhat for SEM-EDAX analysis.

References

1. P. L. Xavier, K. Chaudhari, A. Baksi and T. Pradeep, *Nano Rev.*, 2012, **3**, 14767 and the references cited there in.
2. J. Zheng, C. Zhang and R. M. Dickson, *Phys. Rev. Lett.*, 2004, **93**, 077402/077401-077404.
3. J. Zheng, P. R. Nicovich and R. M. Dickson, *Annu. Rev. Phys. Chem.*, 2007, **58**, 409-431.
4. R. Jin, *Nanoscale*, 2012, **2**, 343-362.
5. G. C. Bond, C. Louis, D. T. Thompson and Editors, *Catalysis by Gold*, World Scientific, 2006.
6. M. Zhu, E. Lanni, N. Garg, M. E. Bier and R. Jin, *J. Am. Chem. Soc.*, 2008, **130**, 1138-1139.
7. M. Zhu, C. M. Aikens, F. J. Hollander, G. C. Schatz and R. Jin, *J. Am. Chem. Soc.*, 2008, **130**, 5883-5885.
8. Y. Shichibu, Y. Negishi, T. Tsukuda and T. Teranishi, *J. Am. Chem. Soc.*, 2005, **127**, 13464-13465.
9. E. S. Shibu, M. A. H. Muhammed, T. Tsukuda and T. Pradeep, *J. Phys. Chem. C*, 2008, **112**, 12168-12176.
10. Y. Negishi, K. Nobusada and T. Tsukuda, *J. Am. Chem. Soc.*, 2005, **127**, 5261-5270.
11. M. W. Heaven, A. Dass, P. S. White, K. M. Holt and R. W. Murray, *J. Am. Chem. Soc.*, 2008, **130**, 3754-3755.
12. A. Dass, *J. Am. Chem. Soc.*, 2009, **131**, 11666-11667.
13. Z. Wu, J. Suhan and R. Jin, *J. Mater. Chem.*, 2009, **19**, 622-626.
14. L. A. Angel, L. T. Majors, A. C. Dharmaratne and A. Dass, *ACS Nano*, 2010, **4**, 4691-4700.
15. J. Akola, K. A. Kacprzak, O. Lopez-Acevedo, M. Walter, H. Gronbeck and H. Hakkinen, *J. Phys. Chem. C*, 2010, 114, 15986-15994.
16. O. Toikkanen, V. Ruiz, G. Ronnholm, N. Kalkkinen, P. Liljeroth and B. M. Quinn, *J. Am. Chem. Soc.*, 2008, **130**, 11049-11055.
17. H. Qian, M. Zhu, U. N. Andersen and R. Jin, *J. Phys. Chem. A*, 2009, **113**, 4281-4284.
18. Y. Pei, Y. Gao and X. C. Zeng, *J. Am. Chem. Soc.*, 2008, 130, 7830-7832.
19. O. Lopez-Acevedo, H. Tsunoyama, T. Tsukuda, H. Hakkinen and C. M. Aikens, *J. Am. Chem. Soc.*, 2010, **132**, 8210-8218.
20. J. Kim, K. Lema, M. Ukaigwe and D. Lee, *Langmuir*, 2007, **23**, 7853-7858.
21. V. L. Jimenez, D. G. Georganopoulou, R. J. White, A. S. Harper, A. J. Mills, D. Lee and R. W. Murray, *Langmuir*, 2004, **20**, 6864-6870.
22. R. L. Donkers, D. Lee and R. W. Murray, *Langmuir*, 2008, **24**, 5976.
23. H. Qian, W. T. Eckenhoff, Y. Zhu, T. Pintauer and R. Jin, *J. Am. Chem. Soc.*, 2010, **132**, 8280-8281.
24. P. D. Jadzinsky, G. Calero, C. J. Ackerson, D. A. Bushnell and R. D. Kornberg, *Science* 2007, **318,** 430-433.
25. Y.-K. Han, H. Kim, J. Jung and Y. C. Choi, *J. Phys. Chem. C*, 2010, **114**, 7548-7552.
26. C. Zeng, H. Qian, T. Li, G. Li, N. L. Rosi, B. Yoon, R. N. Barnett, R. L. Whetten, U. Landman and R. Jin, *Angew. Chem., Int. Ed.*, 2012, **51**, 13114-13118.

27. Y. Negishi, W. Kurashige, Y. Niihori, T. Iwasa and K. Nobusada, *Phys. Chem. Chem. Phys.*, 2010, **12**, 6219-6225.
28. Y. Negishi, K. Igarashi, K. Munakata, W. Ohgake and K. Nobusada, *Chem. Commun.*, 2012, **48**, 660-662.
29. J. Xie, Y. Zheng and J. Y. Ying, *J. Am. Chem. Soc.*, 2009, **131**, 888-889.
30. M. M. A. Habeeb, P. K. Verma, S. K. Pal, A. Retnakumari, M. Koyakutty, S. Nair and T. Pradeep, *Chem. - Eur. J.*, 2010, **16**, 10103-10112.
31. A. Mathew, P. R. Sajanlal and T. Pradeep, *J. Mater. Chem.*, 2010, **21**, 11205-11212.
32. C. V. Durgadas, C. P. Sharma and K. Sreenivasan, *Analyst* 2010, **136**, 933-940.
33. D. Hu, Z. Sheng, P. Gong, P. Zhang and L. Cai, *Analyst*, 2010, **135**, 1411-1416.
34. C. Guo and J. Irudayaraj, *Anal. Chem.*, 2011, **83**, 2883-2889.
35. H.-W. Li, K. Ai and Y. Wu, *Chem. Commun.*, 2011, **47**, 9852-9854.
36. J. S. Mohanty, P. L. Xavier, K. Chaudhari, M. S. Bootharaju, N. Goswami, S. K. Pal and T. Pradeep, *Nanoscale*, 2012, **4**, 4255-4262.
37. P. L. Xavier, K. Chaudhari, P. K. Verma, S. K. Pal and T. Pradeep, *Nanoscale*, 2010, **2**, 2769-2776.
38. K. Chaudhari, P. L. Xavier and T. Predeep, *ACS Nano*, 2011, **5**, 8816-8827.
39. H. Wei, Z. Wang, L. Yang, S. Tian, C. Hou and Y. Lu, *Analyst* 2010, **135**, 1406-1410.
40. Y.-H. Lin and W.-L. Tseng, *Anal. Chem.*, 2010, **82**, 9194-9200.
41. W.-Y. Chen, J.-Y. Lin, W.-J. Chen, L. Luo, D. E. Wei-Guang and Y.-C. Chen, *Nanomedicine* 2010, **5**, 755-764.
42. T.-H. Chen and W.-L. Tseng, *Small*, 2012, **8**, 1912-1919.
43. A. Baksi, P. L. Xavier, K. Chaudhari, N. Goswami, S. K. Pal and T. Pradeep, *Nanoscale*, 2013, **5**, 2009-2016.
44. A. Baksi, T. Pradeep, B. Yoon, C. Yannouleas and U. Landman, *ChemPhysChem*, 2013, **14**, 1272-1282 and the references cited there in.
45. C.-L. Liu, H.-T. Wu, Y.-H. Hsiao, C.-W. Lai, C.-W. Shih, Y.-K. Peng, K.-C. Tang, H.-W. Chang, Y.-C. Chien, J.-K. Hsiao, J.-T. Cheng and P.-T. Chou, *Angew. Chem., Int. Ed.*, 2011, **50**, 7056-7060.
46. N. Goswami, A. Giri, M. S. Bootharaju, P. L. Xavier, T. Pradeep and S. K. Pal, *Anal. Chem.* , 2011, **83**, 9676-9680.
47. Y.-C. Shiang, C.-C. Huang, W.-Y. Chen, P.-C. Chen and H.-T. Chang, *J. Mater. Chem.*, 2012, **22**, 12972-12982.
48. S. M. Lystvet, S. Volden, G. Singh, M. Yasuda, O. Halskau and W. R. Glomm, *RSC Adv.*, 2013, **3**, 482-495.
49. S. M. Lang, A. Frank, I. Fleischer and T. M. Bernhardta, *Eur. Phys. J. D*, 2013, **67**, 19.
50. D. W. Yuan, Y. Wang and Z. Zeng, *J. Chem. Phys.*, 2005, **122**, 114310/114311-114311.
51. D. M. Popolan, M. Noessler, R. Mitric, T. M. Bernhardt and V. Bonacic-Koutecky, *Phys. Chem. Chem. Phys.*, 2011, **12,** 7865-7873.
52. T. M. Bernhardt, J. Hagen, S. M. Lang, D. M. Popolan, L. D. Socaciu-Siebert and L. Woste, *J. Phys. Chem. A*, 2009, **113**, 2724-2733.
53. H. J. De, N. Veldeman, P. Claes, E. Janssens, M. Andersson and P. Lievens, *J. Phys. Chem. A*, 2011, **115**, 2103-2109.
54. Y. Negishi, K. Munakata, W. Ohgake and K. Nobusada, *J. Phys. Chem. Lett.*, 2012, **3**, 2209-2214.
55. W. E. Kaden, T. Wu, W. A. Kunkel and S. L. Anderson, *Science* 2009, **326**, 826-829.

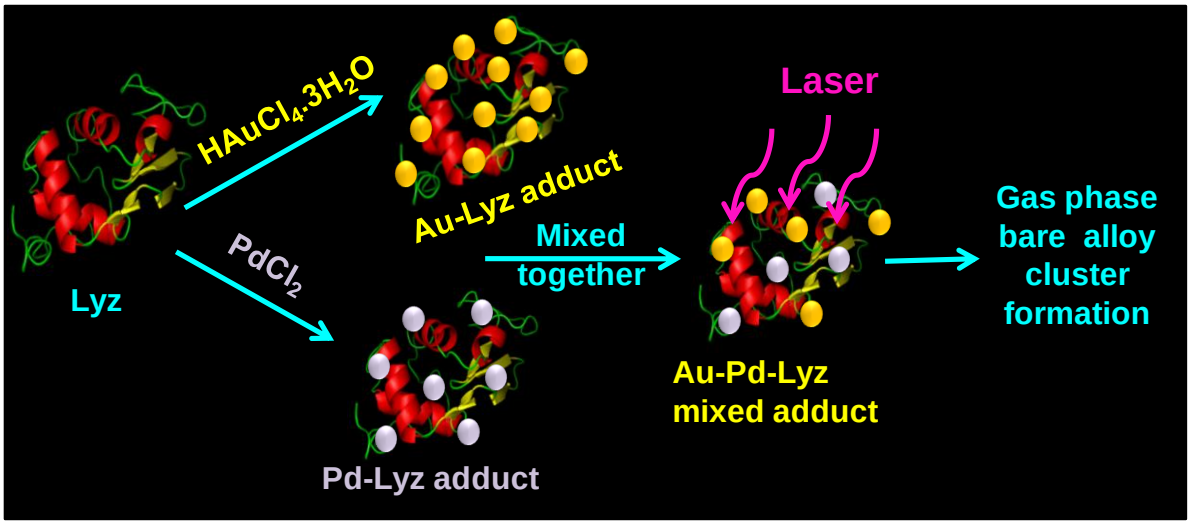

Table of content graphic

Figure 1

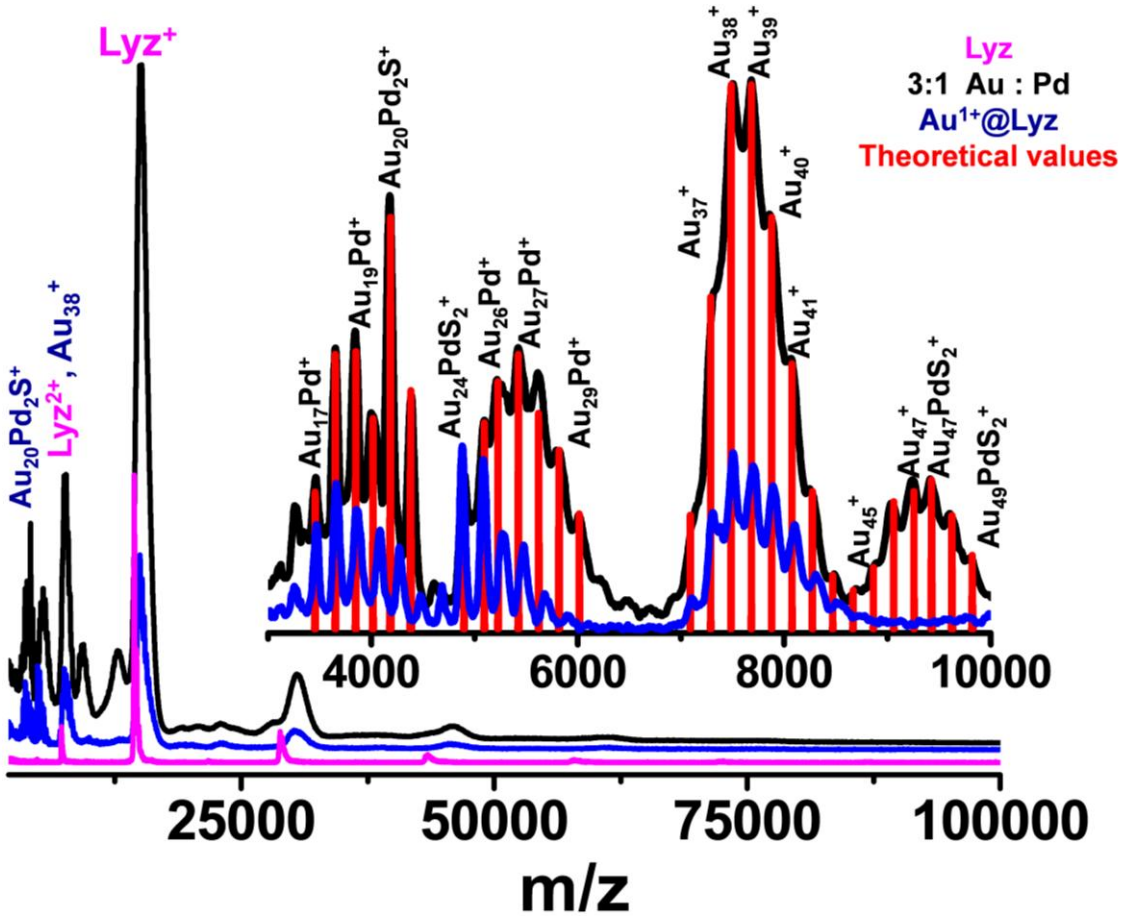

Fig. 1 MALDI MS study of Au and Au-Pd adducts of Lyz in the positive ion mode in the range of 2000-100000 Da. The 3000-10000 Da region has been expanded in the inset. Au-Pd adducts show distinctly different features compared to Au-alone adducts, due to the formation of alloys. The assigned peaks match well with the theoretical values.

Figure 2

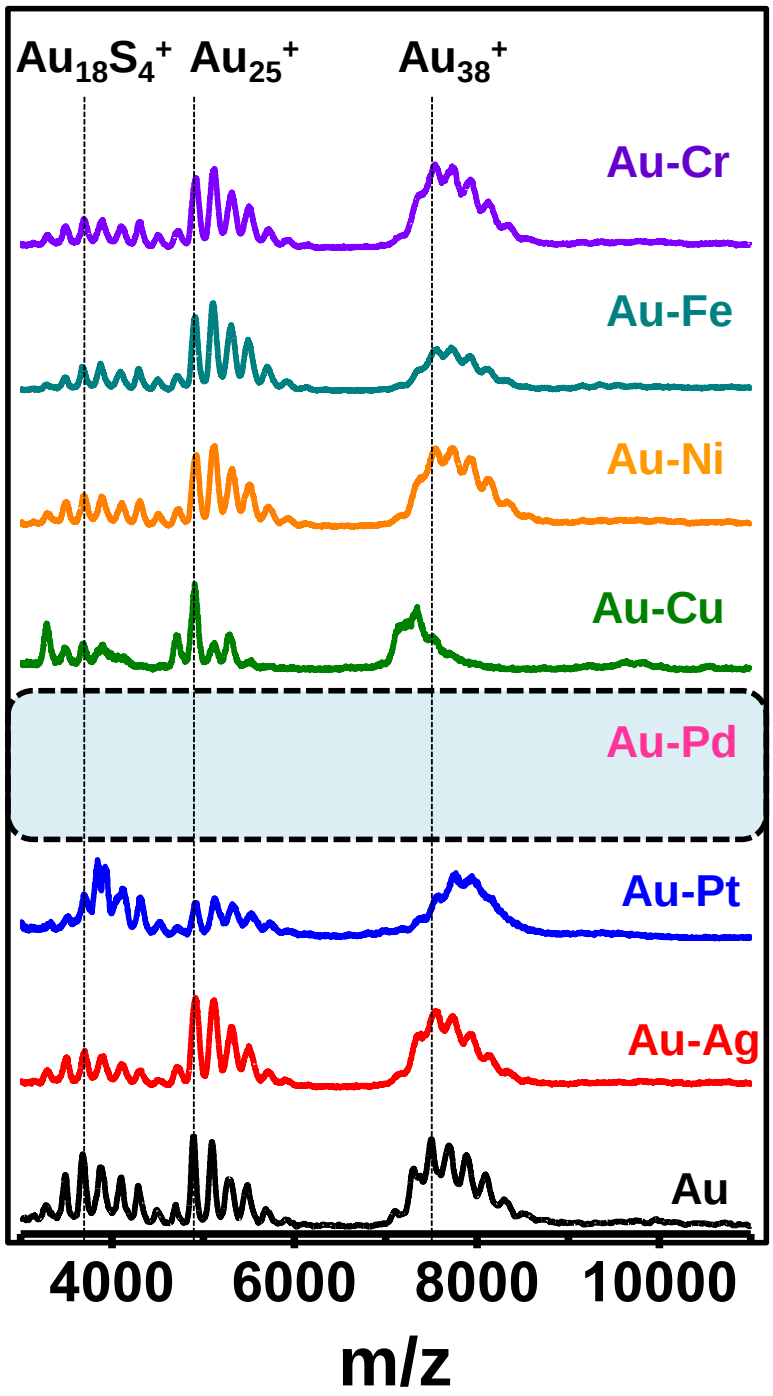

Fig. 2 MALDI MS study of the effect of metal ions on gas phase alloy formation. 3d, 4d and 5d metal ions, known to form alloys with gold are chosen for this study. All the concentration ratios of Au and M-adducts are same. Mixed adducts of gold and individual metal have been used for this study. Only Pd shows distinct alloy formation, which has been highlighted.

Figure 3

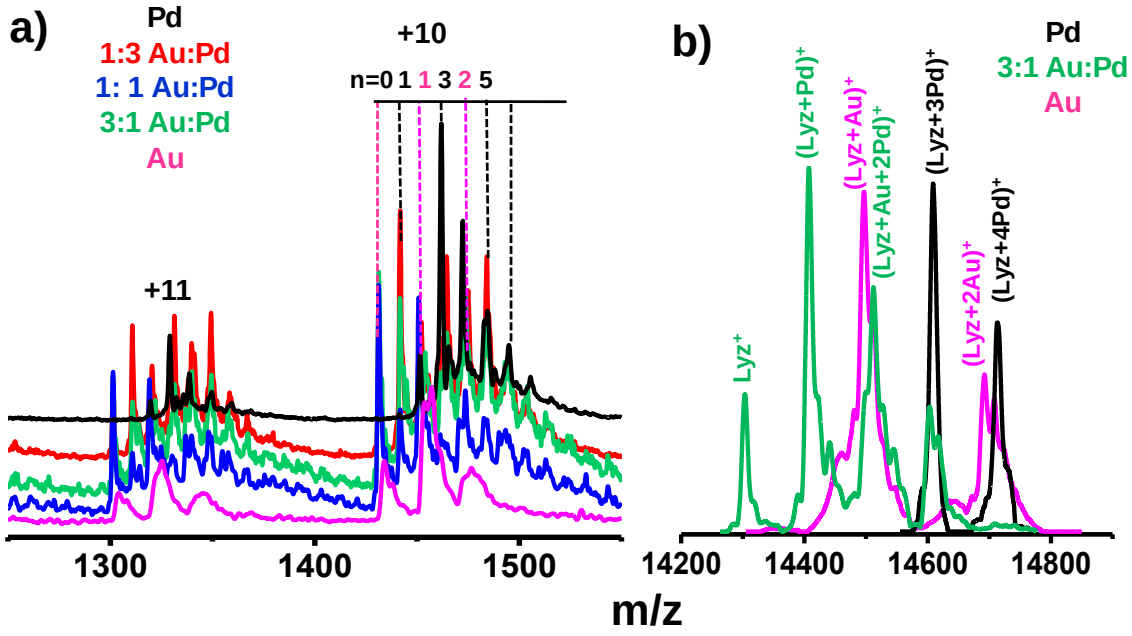

Fig. 3 *a)* ESI MS of Au, Pd and Au-Pd mixed adducts of Lyz showing individual peaks due to Au and Pd attachments. In the mixture, Au and Pd attachment peaks are seen. b) Deconvoluted spectra of Au, Pd and mixed adducts of Lyz. The 3:1 Au:Pd adduct is showing peaks due to simultaneous attachment of Au and Pd.

Figure 4

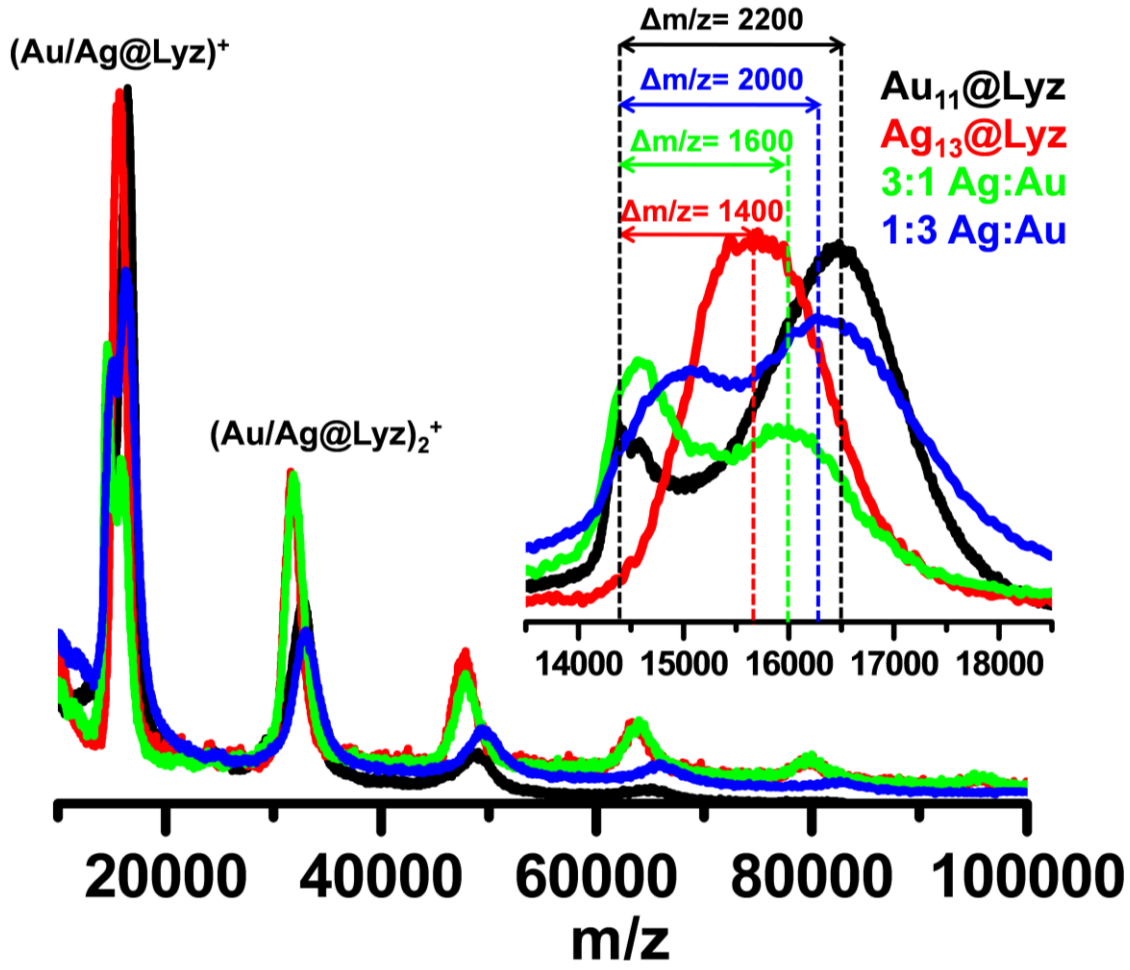

Fig. 4 MALDI MS of Au_{QCs}@Lyz, Ag_{QCs}@Lyz and Au-Ag_{QCs}@Lyz in the linear positive mode showing distinct separation from the parent protein peak due to specific number of Au and Ag. Monomer region is expanded in the inset showing tunable alloy formation by varying the Au and Ag precursor concentrations.

Figure 5

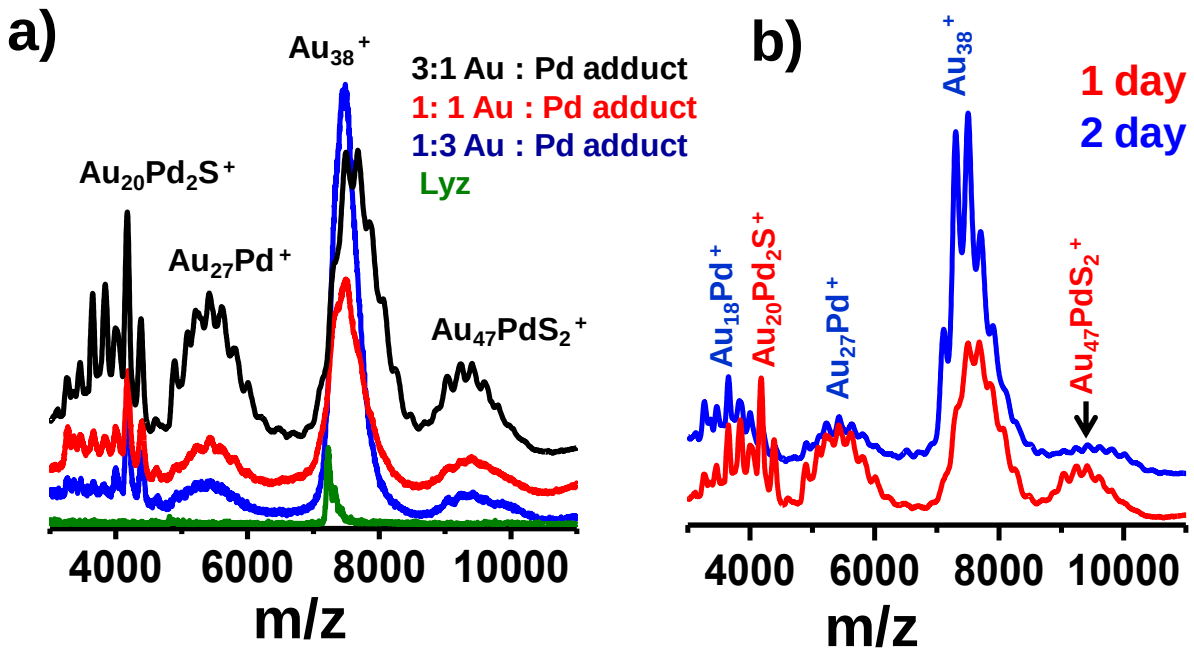

Fig. 5 *a)* Concentration dependent study of different Au:Pd adducts of Lyz. 3:1 Au:Pd adduct of Lyz shows good intensity and resolvable peak separation. b) Time dependent study of 3:1 Au:Pd adduct of Lyz showing catalytic enhancement of Au_{38}^{+} over incubation time.

Figure 6

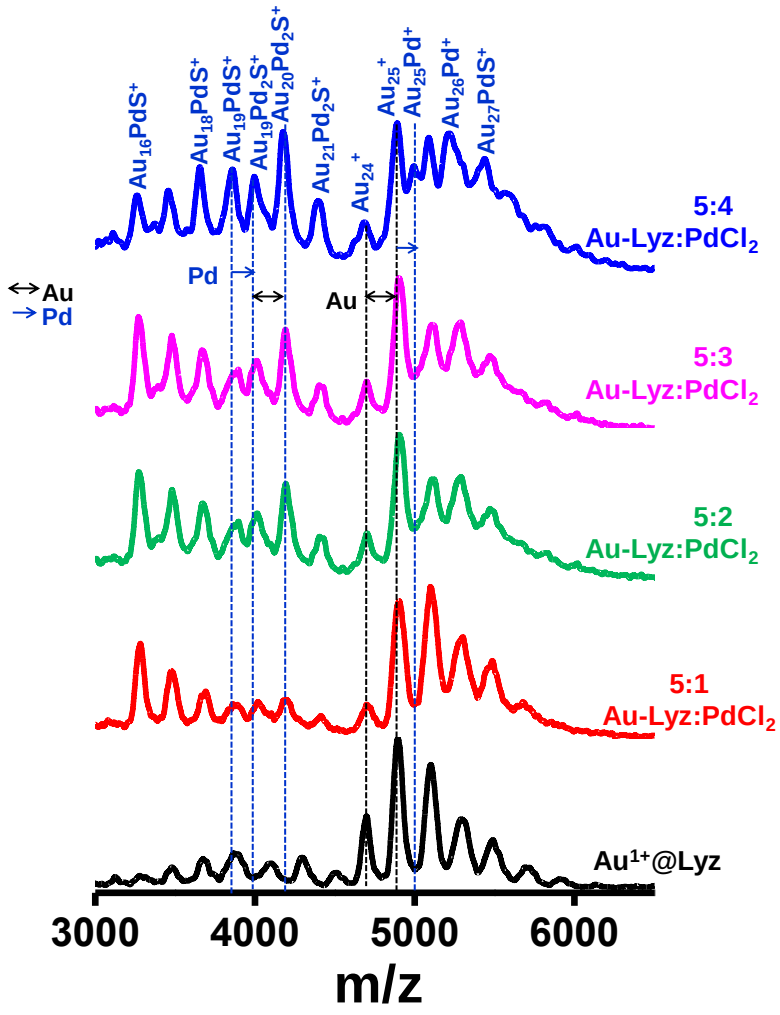

Fig. 6 Effect of direct $PdCl_2$ addition to Au-Lyz adducts probed by MALDI MS with different Au-Lyz:$PdCl_2$ ratios (as mentioned on the traces). With minimum $PdCl_2$ addition, alloy forms as observed in the Au_{18}^+ region but the Au_{25}^+ region remains unchanged. In the case of highest Au-Lyz:$PdCl_2$ ratio, alloy formation is observed with a few sulfur attachments.

Figure 7

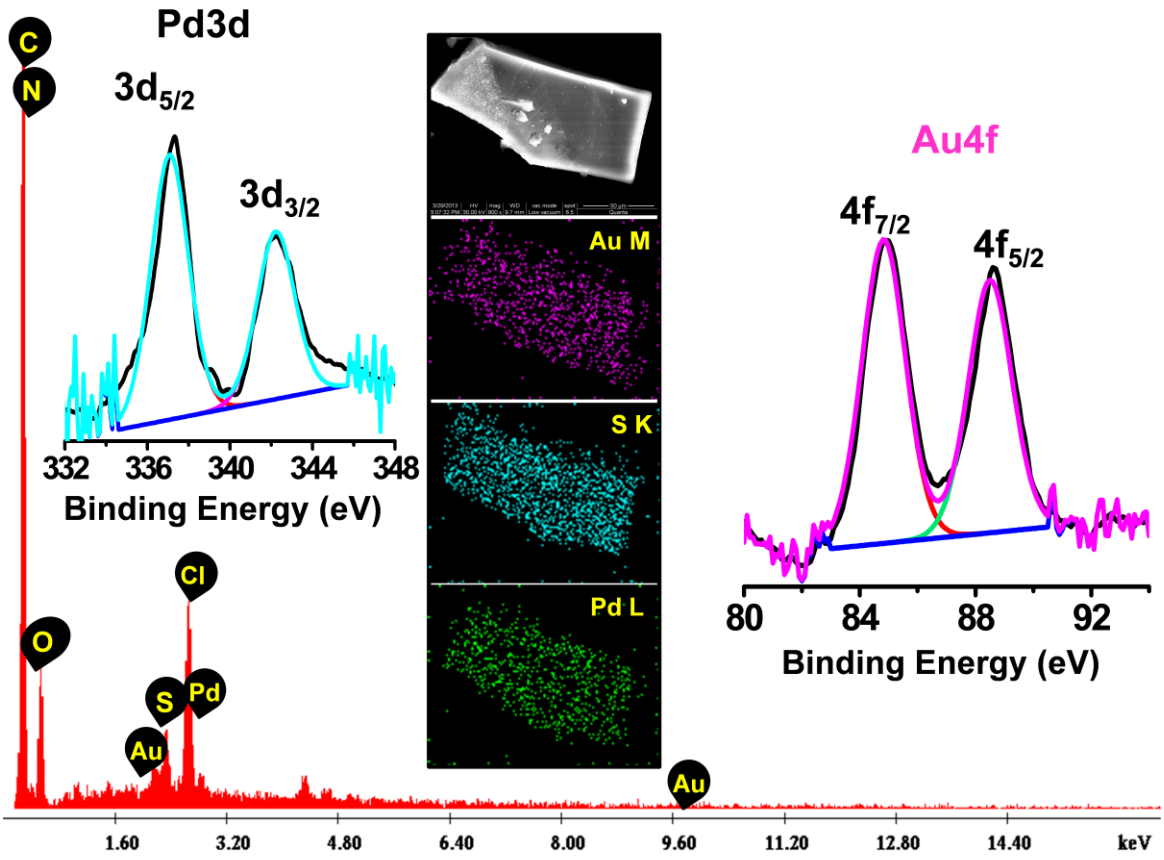

Fig. 7 SEM-EDAX of 3:1 Au:Pd adduct of Lyz, showing presence of all possible elements. Inset i) shows the EDAX mapping of the object shown in SEM image at the top. A) and B) are XPS spectra of Au-Lyz and Pd-Lyz adducts showing that Au^{3+} is reduced to Au^{1+} after adduct formation with protein, whereas Pd^{2+} remains in the same oxidation state.

Figure 8

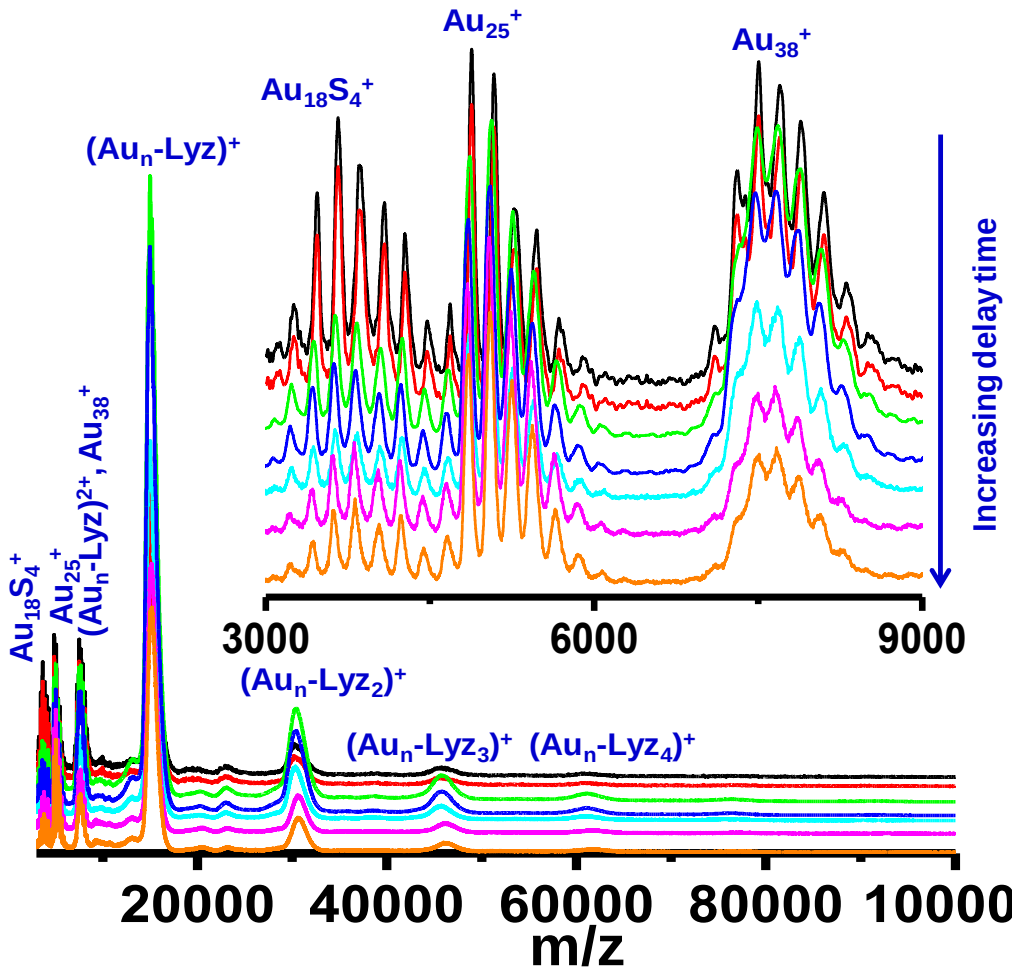

Fig. 8 MALDI MS spectra of delay time dependent bare cluster formation of Au^{+}@Lyz. There is no signature of any new cluster core formation with varying delay time. Inset shows an expanded view of m/z 3000 to 9000. With changing delay time no new peak appears.